A Numerical Modeling Study on the Earth's Surface Brightening Effect of Cirrus Thinning

Xiangjun Shi *, Yuxin Liu , Jiaojiao Liu

Posted Date: 11 December 2023

doi: 10.20944/preprints202312.0733.v1

Keywords: cirrus cloud thinning; seeding method; brightening effect; cooling effect

Article

A Numerical Modeling Study on the Earth's Surface Brightening Effect of Cirrus Thinning

Xiangjun Shi*, Yuxin Liu and Jiaojiao Liu

School of Atmospheric Sciences, Nanjing University of Information Science and Technology, Nanjing 210044, China; liuyuxin@nuist.edu.cn (Y.L.); liujj@nuist.edu.cn (J.L.)

* Correspondence: shixj@nuist.edu.cn

Abstract: Cirrus thinning, as one kind of geoengineering approach, not only cools our planet but also enhances the amount of sunlight reaching Earth's surface (brightening effect). This study delves into the brightening effect induced by cirrus thinning with a flexible seeding method. The thinning of cirrus clouds alone leads to a considerable globally averaged cooling effect (−2.46 W m^{-2}), along with a notable globally averaged brightening effect (2.19 W m^{-2}). Cirrus thinning also results in substantial reductions in the cloud radiative effects of the lower mixed-phase and liquid clouds. While these reductions counteract the cooling effect from cirrus clouds, they enhance the brightening effect from cirrus clouds. Consequently, the brightening effect caused by cirrus seeding (4.69 W m^{-2}) is considerably more potent than its cooling effect (−1.21 W m^{-2}). Furthermore, due to the more pronounced changes from the mixed-phase and liquid clouds at low- and mid-latitudes, the cooling effect is primarily concentrated at high latitudes. In contrast, the brightening effect is significantly stronger over most low- and mid-latitude regions. Overall, cirrus thinning could lead to a notable brightening effect, which can be leveraged to offset the dimming effect (the opposite of brightening effect) of other geoengineering approaches.

Keywords: cirrus cloud thinning; seeding method; brightening effect; cooling effect

1. Introduction

Geoengineering, considered as a supplementary strategy to counteract global warming, has been garnering more and more attention in recent years [1–8]. Geoengineering approaches can be briefly divided into two categories: carbon dioxide removal (CDR) and solar radiation modification (SRM) [9–14]. CDR techniques aim to remove CO2 directly from the atmosphere by either increasing natural sinks for carbon or using physical/chemical engineering to remove the CO2 [15–18]. SRM techniques aim to modify the Earth's radiation budget through artificial intervention, such as stratospheric aerosol injection, marine cloud brightening, and cirrus cloud thinning [19–24]. Compared to CDR techniques, more attention is paid to SRM techniques due to their relatively low cost and faster cooling effects [25–29].

SRM techniques are often referred to as "Plan B", "last-ditch response", or "emergency shield" due to the uncertain potential side effects and risks [30–34]. Previous studies have pointed out that SRM techniques could affect extreme precipitation events and ecological systems [35–40]. For instance, stratospheric aerosol injection significantly impacts the frequency of tropical cyclones [41]. Moreover, cirrus thinning might lead to more vigorous convective activities [42,43]. Among all potential ecological influences, the most significant might be on food production. Climate intervention could impact food crop production in several ways, including insolation effect, hydrological effect, and heat stress. The impacts and risks would vary depending on the specific SRM technique used and the types of crops involved. Therefore, results vary greatly between different studies [44–50]. Overall, our understanding of the SRM side effects is still in its early stages. In order to gain confidence about geoengineering deployments, it's crucial that we conduct in-depth evaluations of the benefits and harms associated with using SRM techniques [51–54].

 doi:10.20944/preprints202312.0733.v1

Cirrus clouds typically reflect a smaller amount of incoming solar radiation, yet they trap a larger proportion of Earth's outgoing longwave radiation, thereby contributing to the warming of our planet [55–57]. Cirrus thinning techniques cool the Earth by allowing more longwave radiation to escape into space, while most SRM techniques (e.g., stratospheric aerosol injection and marine cloud brightening) cool the Earth by reflecting more solar radiation back into space [58–60]. Unlike solar dimming techniques, cirrus thinning could increase the amount of sunlight reaching Earth's surface [61,62]. This would be referred to as a 'brightening effect' in this study. The sunlight at Earth's surface plays an important role in photosynthesis, which is vital for plant growth and ecological systems [63–67]. However, there are few studies focused on the brightening effect of cirrus thinning and its corresponding mechanisms.

The present study aims to better estimate the brightening effect caused by cirrus thinning via a flexible seeding method. Compared to the cirrus thinning method (i.e., artificially increasing the sedimentation velocity of cloud particles) proposed in Phase 6 of the Geoengineering Model Intercomparison Project (GeoMIP6; [26]), the seeding method is relatively more physically feasible, and its corresponding simulation results offer superior reference values. The structure of this study is as follows: the seeding method and experimental design are described in Section 2; the simulation results are presented and analyzed in Section 3; finally, the discussion is presented in Section 4, and the conclusions are provided in Section 5.

2. Experiments and Methods

2.1. Two Kinds of Models Used in This Study

To better understand how to make cirrus clouds thinner by a physically feasible approach, a cloud parcel model is employed to demonstrate the process of thinning cirrus clouds. The parcel model showcases the process of ice crystals (ICs) formation within an adiabatically rising air parcel, which maintains a constant updraft vertical velocity (W). ICs formation process considers the competition between homogeneous nucleation on soluble aerosol particles and heterogeneous nucleation on ice nuclei particles (INPs, insoluble aerosol particles). Equations that outline the evolution of temperature (T), pressure (P), ice-phase supersaturation (S_i), and ICs size (R_i) are well-documented in academic textbooks (e.g., [68]). For more detailed information about this cloud parcel model, please refer to the work by Shi and Liu (2016) [69].

The Community Atmosphere Model version 5.3 (CAM5; [70]) is used to carry out climate simulations. In CAM5, cloud microphysics is represented by a two-moment scheme [71]. Besides the default ice nucleation parameterizations developed by Liu and Penner in 2005 (hereafter LP), the ICs formation process can also be represented by the ice nucleation parameterizations developed by Barahona and Nenes in 2009 (hereafter BN) [72,73]. The newly formed ICs number concentration (N_{inuc}) is mainly dependent on effective sub-grid vertical velocity (W_{eff}), the number concentration of coarse-mode dust aerosols (N_{dust}, which can 100% act as INPs) and the number concentration of sulfate aerosols (N_{sul}, soluble particles) [74]. In mixed-phase clouds (0 ℃ ≥ T > −37 ℃), only heterogeneous nucleation occurs. Besides the ice nucleation process, the detrainment from convective activity is also a source for ICs. Finally, it is necessary to point out that cirrus cloud is referred to ice cloud (T < −37 ℃) in cloud microphysics scheme [10,75].

2.2. A Physically Feasible Method used for Cirrus Thinning

Under the condition for cirrus cloud formation, heterogeneous nucleation occurs earlier with the aid of INPs. Usually, heterogeneous nucleation only produces a limited number of ICs (less than 100 L^{-1}). This is primarily due to the relatively low concentration of INPs (N_{INP}) in the upper troposphere. The threshold S_i for homogeneous nucleation (S_{ihom}, usually >50%) is relatively higher. In other words, it is difficult to achieve homogeneous nucleation. However, homogeneous nucleation can produce a large number of ICs, typically much greater than 100 L^{-1}. This is primarily due to the high concentration of soluble aerosols present in the environment [76,77]. Therefore, decreasing in-cloud ICs number concentration (N_i) can be achieved by preventing homogeneous nucleation from

Preprints (www.preprints.org) | NOT PEER-REVIEWED | Posted: 11 December 2023 doi:10.20944/preprints202312.0733.v1

occurring [58,78]. If the INPs could reach a certain number concentration (N_{INPlim}, usually less than 100 L^{-1}), the ICs from heterogeneous freezing could prevent S_i from reaching S_{ihom} because these new-formed ICs consume water vapor via deposition growth [73,79]. In other words, cirrus thinning (i.e., decreasing N_i and cloud optical depth) can be achieved by seeding with a few INPs ($N_{INPseed} = N_{INPlim} - N_{INP}$, if $N_{INP} < N_{INPlim}$).

Figure 1 illustrates three different ICs formation processes from parcel model simulations. In the reference simulation (REF, black lines), heterogeneous nucleation produces 10 L^{-1} ICs when S_i reaches ~10%. Afterward, S_i is still increasing because these new-formed ICs are too few. Finally, homogeneous nucleation takes place (i.e., S_i reaches S_{ihom}) and produces 2937 L^{-1} ICs. The simulation that only heterogeneous nucleation is allowed (HET, green lines) can be viewed as an idealized method of cirrus thinning, indicating the maximum potential effect of decreasing N_i (decreases to 10 L^{-1}). In the simulation involving seeding with 35 L^{-1} (i.e., $N_{INPseed}$) of INPs (SEED, red lines), the 45 L^{-1} (i.e., N_{INPlim}) ICs produced by heterogeneous freezing can prevent S_i from reaching S_{ihom}. As a result, the final N_i is still 45 L^{-1}. It's evident that the final N_i from the SEED simulation is significantly decreased as compared to the REF simulation. The BN ice nucleation parameterization provides the minimum INPs number concentration (i.e., N_{INPlim}), which could hinder homogeneous nucleation. This is the reason why the BN parameterization is implemented in CAM5.

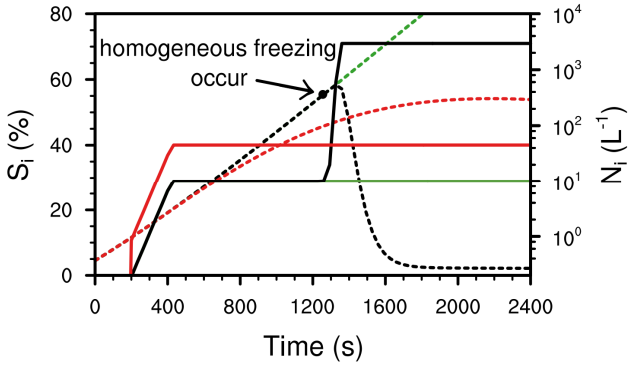

Figure 1. Schematic diagram of cirrus thinning methods. Shown are reference simulation without seeding (REF, black), seeding INPs simulation (SEED, red), and only heterogeneous nucleation simulation (HET, green). The ice supersaturation (S_i, units: %) and number concentration of ice crystals (ICs) (N_i, units: L^{-1}) in the air parcel are represented by dashed and solid lines, respectively. All simulations start with common initial conditions (N_{INP} =10 L^{-1}, N_{sul} = 500 000 L^{-1}, P = 330 hPa, T = 220 K, and W = 0.3 m s^{-1}).

2.3. Climate Simulation Setup

In alignment with the three parcel model simulations previously discussed, there exist three corresponding climate simulations conducted using CAM5. As compared to the REF simulation, the homogeneous nucleation is artificially deactivated in the HET simulation (i.e., pure heterogeneous nucleation). In the SEED simulation, if $N_{dust} < N_{INPlim}$, a specific number (i.e., $N_{INPseed}$) of INPs is incorporated into the coarse-mode dust aerosols (i.e., INPs) used for driving ice nucleation parameterization. It is noteworthy that the changes in cirrus clouds, directly resulting from cirrus thinning, would also exert an influence on the lower mixed-phase and liquid clouds [4,32,43,80]. To enhance the analysis of how cirrus thinning affects radiative fluxes, some modifications have been made to the radiation package. Besides the default entire cloud optical depth (COD) and cloud radiative effect (CRE, the difference in the radiative fluxes between the cloud and cloud-free atmosphere), the radiation package also diagnoses COD and CRE specifically for cirrus clouds (iCOD and iCRE). Meanwhile, COD and CRE from mixed-phase and liquid clouds (mlCOD and mlCRE) are calculated by subtracting iCOD from COD, and iCRE from CRE.

All climate simulations (i.e., REF, HET, and SEED) are atmosphere-only simulations (i.e., sea surface temperature and sea ice are given) with a horizontal resolution of 1.9° latitude × 2.5° longitude and 30 vertical layers. All simulations are executed for 11 years, and the last 10 years are used in

 doi:10.20944/preprints202312.0733.v1

analyses. Variability analysis of simulation results is performed using standard deviations, which are calculated based on the averages from each year.

3. Results

To enhance comprehension of the brightening effect induced by cirrus thinning, it is better to illustrate a comparative analysis between this brightening effect and corresponding cooling effect. To facilitate communication, the symbol "Δ" is employed to represent the discrepancies ("△") in relation to the REF simulation from cirrus thinning simulations (HET or SEED). In accordance with previous studies [23,58,81], the cooling effect is quantified by anomalies in CRE at the top of the atmosphere (ΔCRE_{TOA}). Analogous to the cooling effect, the brightening effect is quantified by anomalies in CRE at Earth's surface (ΔCRE_{bri}). It is noteworthy that ΔCRE_{TOA} has longwave (Earth radiation) net flux (including both downward and upward irradiance) and shortwave (solar radiation) net flux (ΔCRE_{TOAlw} and ΔCRE_{TOAsw}) whereas ΔCRE_{bri} solely takes into account the component of downward solar radiation. Here, we not only demonstrate the brightening effect and cooling effect but also place significant emphasis on understanding the corresponding mechanisms. These mechanisms could yield more valuable insights for leveraging the brightening effect.

3.1. Impacts on Cloud Properties

The changes in ICs number concentration caused by cirrus thinning (i.e., both HET and SEED simulations) is analyzed firstly (Figure 2). After artificially turning off homogeneous freezing (i.e., HET simulation), the average number concentration of newly formed ICs under cirrus conditions (N_{inuc}) drastically decreases to a very low level, especially in the Southern Hemisphere where INPs are scarce. Compared to the HET simulation, N_{inuc} is obviously increased in the SEED simulation due to seeding INPs. However, N_{inuc} from the SEED simulation is also much lower than that from the REF simulation. In cirrus clouds, the ICs number concentration (i.e., N_i) is primarily influenced by the process of ice nucleation (i.e., N_{inuc}) [69,74]. As expected, the zonal mean N_i from both HET and SEED simulations is significantly decreased above the –37 ℃ isotherms (i.e., cirrus clouds). All these three simulations show that the N_i in mixed-phase clouds at mid-to-high latitudes is relatively substantial. This might be due to convective detrainment, which provides a lot of ICs. Because there is no homogeneous nucleation in mixed-phase cloud scheme, the N_i in mixed-phase clouds does not significantly decrease in either the HET or SEED simulations. In alignment with the noticeable decrease in N_i (mainly in cirrus clouds), the vertically integrated N_i (i.e., column N_i) also significantly decreases in both HET and SEED simulations. Taken overall, these cirrus thinning simulations have successfully achieved their objective of significantly reducing N_i.

Preprints (www.preprints.org) | NOT PEER-REVIEWED | Posted: 11 December 2023 doi:10.20944/preprints202312.0733.v1

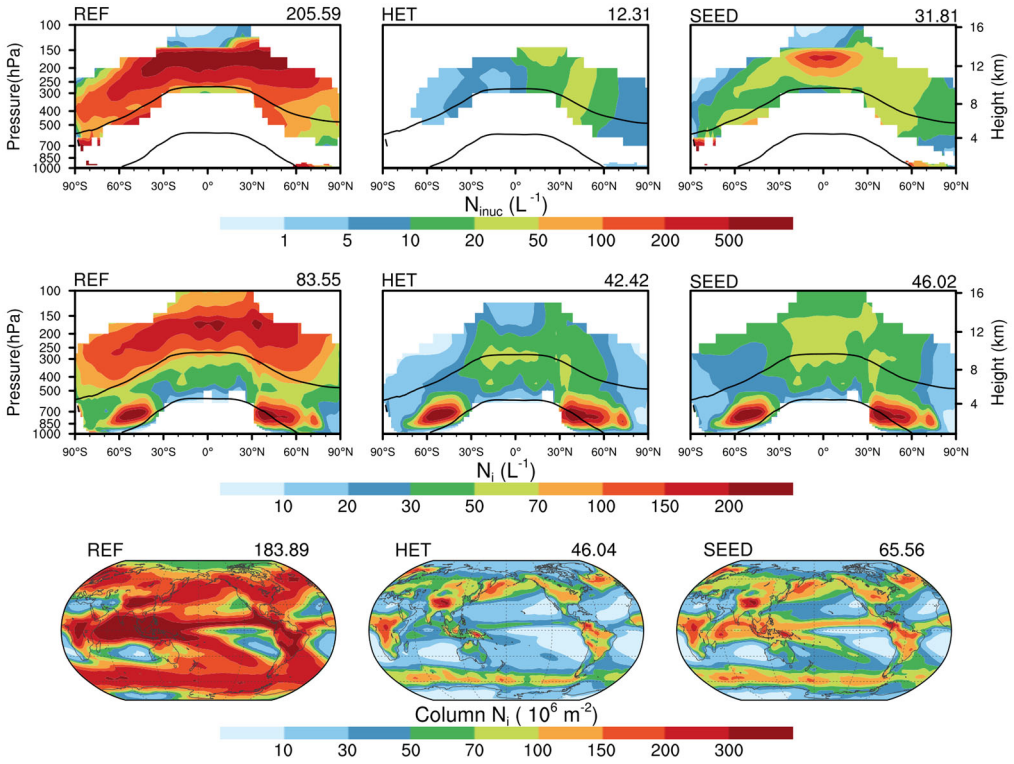

Figure 2. Annual zonal mean of new-formed ICs number concentration in cirrus clouds (N_{inuc}, first row) and in-cloud ICs number concentration (N_i, second row), and spatial distributions of vertically integrated N_i (column N_i, third row). Simulation names and globally averaged values are displayed at the top. The zonal mean results are derived from model grids where the occurrence frequency of corresponding events is greater than 0.1 %. The two black lines denote specific temperatures (0 and –37 °C).

The decrease in N_i (i.e., cirrus thinning) impacts not only the cloud water in cirrus clouds but also the cloud water in mixed-phase and liquid clouds (Figure 3). The ice water content (IWC) in cirrus clouds from both the HET and SEED simulations shows a notable decrease due to lower N_i. Conversely, the IWC in mixed-phase clouds shows an increase across most regions. The main reason might be that cirrus thinning reduces atmospheric stability through its impact on the radiation budget, thereby instigating increased convective activity, which brings more water to mixed-phase cloud layers. The ice water path (IWP) is significantly decreased in most regions because the decrease in IWC in cirrus clouds is stronger than the increase in IWC in mixed-phase clouds. It is worth noting that, in certain regions (e.g., middle Africa and northern Brazil), the IWP is increased because the decreases in IWC within cirrus clouds are slight (which is consistent with the slight decreasing N_i, Figure 2) and these decreases are even less significant than the increases in IWC within mixed-phase clouds there. The liquid water content (LWC) and liquid water path (LWP) are also impacted by the thinning of cirrus clouds, as shown in both HET and SEED simulations. However, these changes in LWC and LWP (i.e., ΔLWC and ΔLWP) are not as noticeable as the ΔIWC and ΔIWP. Despite the overall less noticeable changes in LWC and LWP, it's important to highlight that, in some low- and mid-latitude regions, there are statistically significant decreases in both LWC and LWP. Furthermore, in terms of global mean values, both LWC and LWP are also significantly decreased. One possible reason is that the larger cirrus cloud ICs (associated with cirrus thinning, not shown) fall into the lower mixed-phase and liquid cloud layers and enhances the efficiency of converting cloud droplets into precipitation [59,78]. Another possible reason is that cirrus thinning results in more convective activities and convective precipitation which would consume more cloud water [42,58,59,82]. The above analyses suggest that cirrus thinning also has considerable impacts on the lower mixed-phase and liquid clouds.

Preprints (www.preprints.org) | NOT PEER-REVIEWED | Posted: 11 December 2023 doi:10.20944/preprints202312.0733.v1

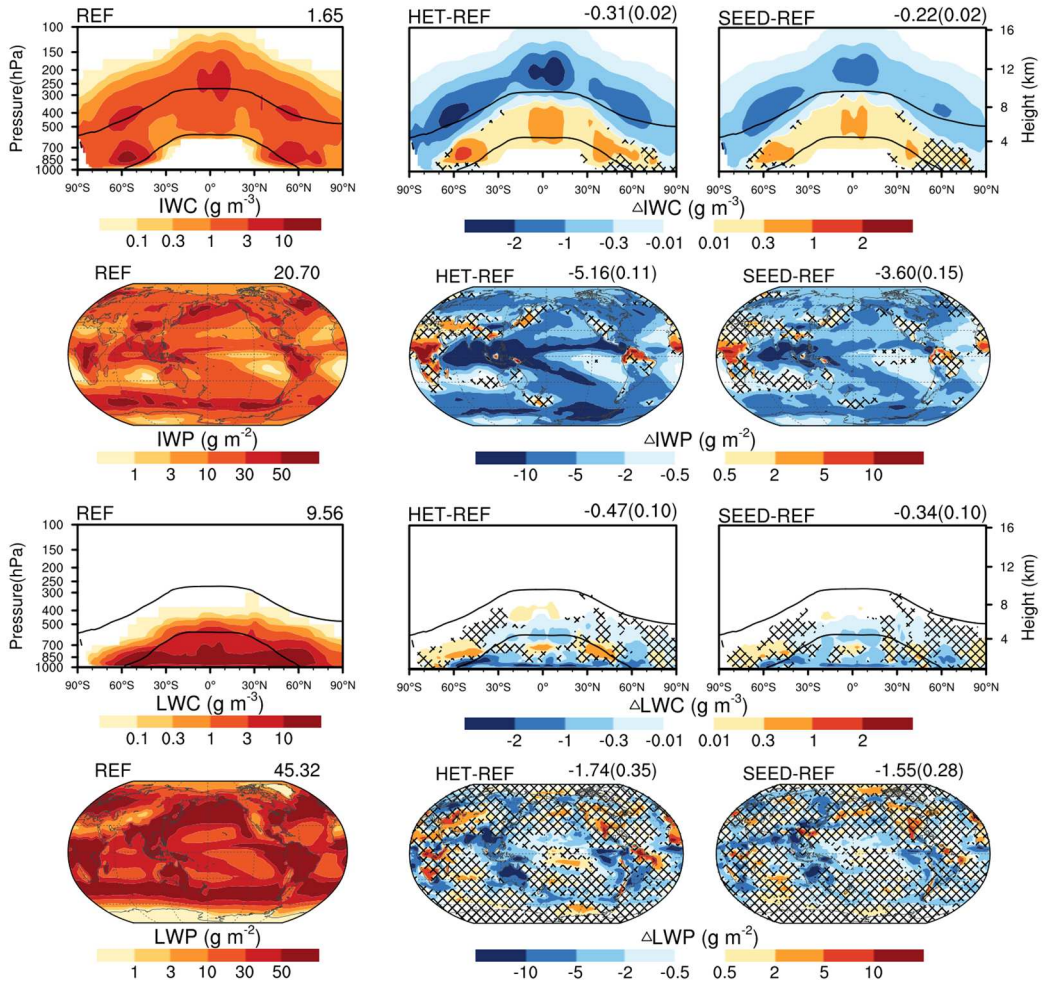

Figure 3. Annual zonal mean ice water content (IWC, first row) and spatial distribution of ice water path (IWP, second row). The third and fourth rows respectively denote the liquid water content (LWC) and the ice water path (IWP). The first column displays the REF simulation, while the second and third columns represent the discrepancies ("Δ") in relation to the REF simulation from both HET and SEED simulations. Global mean values and corresponding standard deviations (in brackets) are shown in the upper right corner. Hatching represents the nonsignificant area at the 90% confidence level.

The changes in CRE mainly depend on the changes in cloud optical depth (COD). Figure 4 shows the changes in COD. Here, the COD in both longwave and shortwave bands (COD_{lw} and COD_{sw}) are shown. Generally, the changes in COD_{lw} and COD_{sw} (i.e., ΔCOD_{lw} and ΔCOD_{sw}) show almost the same special pattern because the change in cloud water is the primary determinant for both COD_{lw} and COD_{sw}. The COD from cirrus clouds (iCOD) is significantly decreased in both longwave and shortwave bands ($iCOD_{lw}$ and $iCOD_{sw}$) over most regions. The global mean values of $iCOD_{lw}$ and $iCOD_{sw}$ are decreased by more than half, especially for the HET simulation. The $\Delta iCOD_{lw}$ and $\Delta iCOD_{sw}$ pass the significance test over most regions except for middle Africa and northern Brazil. Compared to ΔiCOD, the changes in COD from mixed-phase and liquid clouds (ΔmlCOD) become complicated. This is in agreement with the complex changes in cloud water within mixed-phase and liquid clouds (Figure 3). Both $\Delta mlCOD_{lw}$ and $\Delta mlCOD_{sw}$ show statistically significant decreases (i.e., negative values) over some low- and mid-latitude regions. In terms of global mean values, $\Delta mlCOD_{lw}$ is stronger than $\Delta iCOD_{lw}$, and $\Delta mlCOD_{sw}$ is stronger than $\Delta iCOD_{sw}$. In short, cirrus thinning leads to a noticeable and consistent decrease in iCOD across most regions. Additionally, it also results in a substantial reduction in mlCOD over some low- and mid-latitude regions.

Preprints (www.preprints.org) | NOT PEER-REVIEWED | Posted: 11 December 2023 doi:10.20944/preprints202312.0733.v1

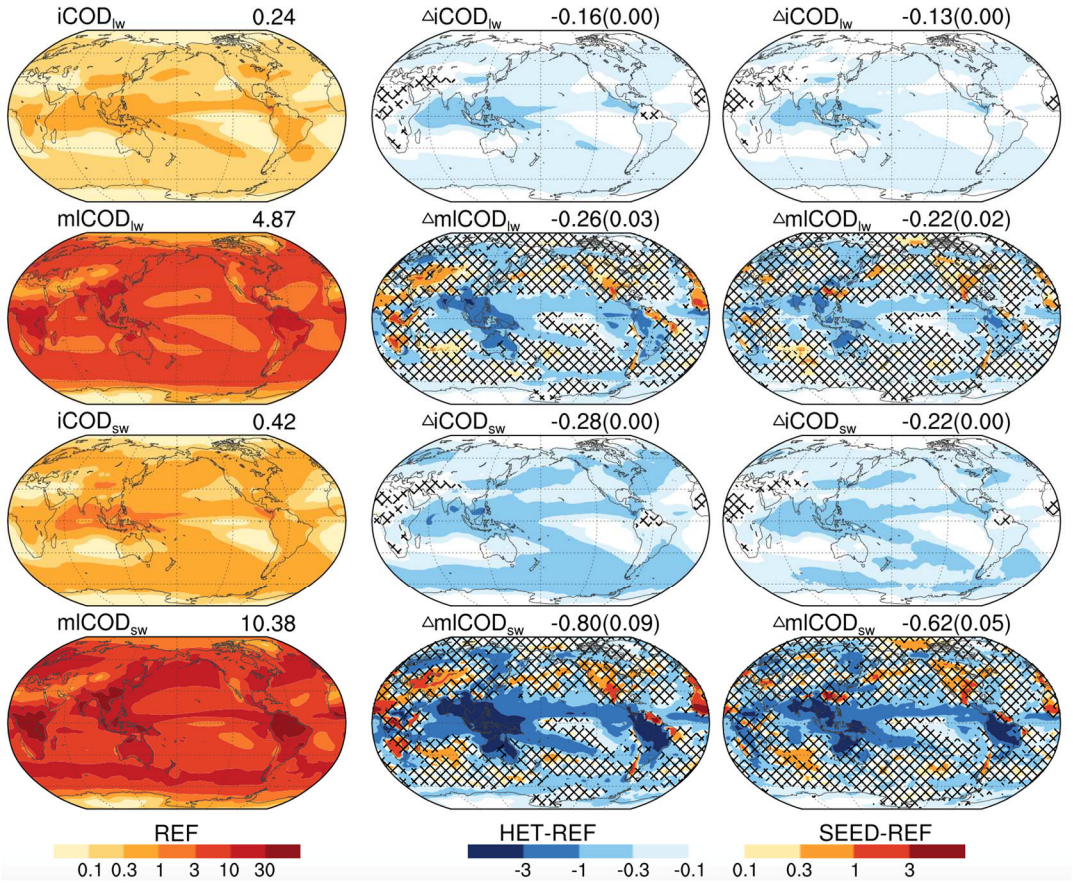

Figure 4. Annual mean maps of cirrus cloud optical depth in longwave band (iCOD$_{lw}$, first row) and shortwave band (iCOD$_{sw}$, third row), and optical depth from mixed-phase and liquid clouds in long-wave band (mlCOD$_{lw}$, second row) and short-wave band (mlCOD$_{sw}$, fourth row).

3.2. Brightening Effect and Cooling Effect

In this section, we quantify the brightening effect and cooling effect of cirrus thinning using CRE$_{bri}$ variables (e.g., ΔCRE$_{bri}$ and ΔmlCRE$_{bri}$) and CRE$_{TOA}$ variables (e.g., ΔiCRE$_{TOA}$ and ΔmlCRE$_{TOA}$), respectively. A positive value of the CRE$_{bri}$ variables indicates a brightening effect, while a negative value suggests the opposite. Similarly, a negative value of the CRE$_{TOA}$ variables signifies a cooling effect and a positive value implies a warming effect.

Firstly, we analyze the CRE$_{TOA}$ variables and CRE$_{bri}$ variables solely from cirrus clouds (Figure 5). The positive iCRE$_{TOAlw}$ indicates that cirrus clouds contribute to the reduction of Earth's outgoing longwave radiation, thereby keeping our planet warm. The negative iCRE$_{TOAsw}$ indicates that cirrus clouds are not conducive to the Earth's absorption of solar radiation, resulting in a cooling effect. Overall, the warming effect (i.e., positive iCRE$_{TOAlw}$) is evidently stronger than the cooling effect (i.e., the absolute value of negative iCRE$_{TOAsw}$). The globally averaged iCRE$_{TOA}$ (iCRE$_{TOAlw}$ + iCRE$_{TOAsw}$) from the REF simulation is 6.53 W m^{-2} (net warming effect). This value falls within the potential range reported in recent studies (4.5 to 6.8 W m^{-2}) [23,32,56,80,83]. The negative iCRE$_{bri}$ suggests that cirrus clouds cause a dimming effect on the Earth's surface. The value of iCRE$_{bri}$ is close to the value of iCRE$_{TOAsw}$, but a little weaker (less negative). This can be explained by that, in the absence of cirrus clouds, more downward solar irradiance can enter the mixed-phase and liquid cloud layers. Although the mixed-phase and liquid clouds scatter and absorb some solar radiation, most of it could reach the Earth's surface causing a brightening effect. All these radiative fluxes (i.e., iCRE$_{TOA}$, iCRE$_{TOAlw}$, iCRE$_{TOAsw}$, and iCRE$_{bri}$) show a similar spatial pattern that aligns with the COD of cirrus clouds (i.e., iCOD$_{lw}$ and iCOD$_{sw}$). After cirrus clouds become thin (i.e., the HET and SEED simulations), the net warming effect and surface dimming effect from cirrus clouds also weaken. In other words, cirrus thinning leads to a cooling and brightening effect. The globally averaged

Preprints (www.preprints.org) | NOT PEER-REVIEWED | Posted: 11 December 2023 doi:10.20944/preprints202312.0733.v1

$\Delta iCRE_{TOA}$ from the HET and SEED simulations are −3.56 ± 0.04 and −2.46 ± 0.04 W m^{-2}, respectively. The globally averaged $\Delta iCRE_{bri}$ from the HET and SEED simulations are 2.78 ± 0.03 and 2.19 ± 0.03 W m^{-2}, respectively. These global mean values suggest that the cirrus cloud net warming effect and surface dimming effect from the REF simulation are reduced by about half. Both the HET and SEED simulations show that the cooling effect (negative $\Delta iCRE_{TOA}$) and brightening effect (positive $\Delta iCRE_{bri}$) are statistically significant over most regions.

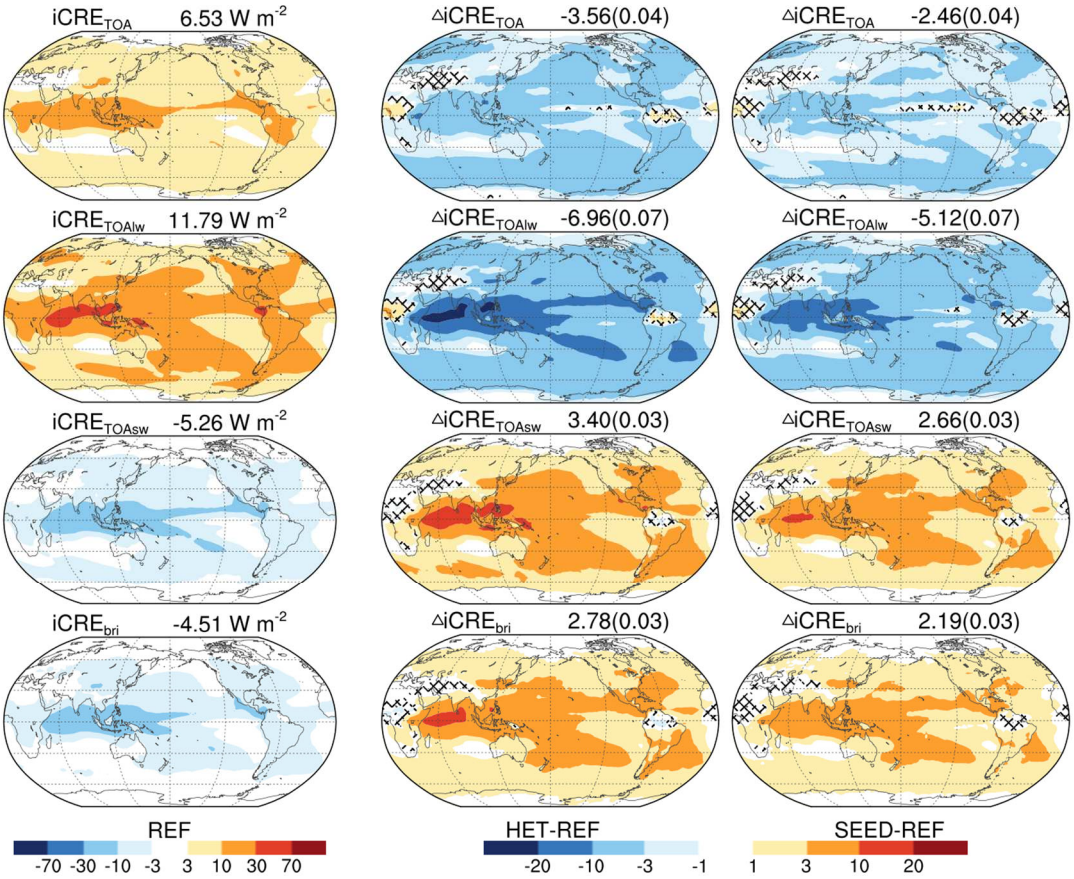

Figure 5. Annual mean maps of cirrus cloud radiative effect ($iCRE_{TOA}$, first row), its longwave ($iCRE_{TOAlw}$, second row) and shortwave ($iCRE_{TOAsw}$, third row) components, and brightness radiative effect ($iCRE_{bri}$, fourth row).

Secondly, the radiative effects of mixed-phase and liquid clouds are analyzed (Figure 6). Similar to cirrus clouds, mixed-phase and liquid clouds also exhibit longwave warming effect (positive $mlCRE_{TOAlw}$) and shortwave cooling effect (negative $mlCRE_{TOAsw}$). Compared to cirrus clouds ($iCRE_{TOAlw}$ and $iCOD_{lw}$), $mlCRE_{TOAlw}$ is only increased by about half despite a roughly twenty-fold increase in $mlCOD_{lw}$. This weaker efficiency (i.e., CRE/COD) primarily stems from the relatively small temperature difference between Earth's surface and these clouds. Unlike $mlCRE_{TOAlw}$, $mlCRE_{TOAsw}$ is approximately ten times stronger than $iCRE_{TOAsw}$. Therefore, the shortwave cooling effect (negative $mlCRE_{TOAsw}$) is much stronger than the longwave warming effect (positive $mlCRE_{TOAlw}$) over most regions. Mixed-phase and liquid clouds show a net cooling effect (negative $mlCRE_{TOA}$). Mixed-phase and liquid clouds also make the Earth's surface dimmer (negative $mlCRE_{bri}$). Here, $mlCRE_{bri}$ (downward solar irradiance at the Earth's surface) is a little stronger (more negative) than $mlCRE_{TOAsw}$ (net radiative flux). The main reason is that a portion of $mlCRE_{bri}$ (surface albedo) is reflected back into the atmosphere. Because the impact of cirrus thinning on mixed-phase and liquid clouds is complex (Figures 3 and 4), the changes in radiative effects caused by cirrus thinning are statistically insignificant over approximately half of the Earth. These two cirrus thinning simulations (i.e., HET and SEED simulations) show that $\Delta mlCRE_{TOAlw}$ is generally negative (cooling effect) and $\Delta mlCRE_{TOAsw}$ is generally positive (warming effect). The positive $\Delta mlCRE_{TOAsw}$ is

Preprints (www.preprints.org) | NOT PEER-REVIEWED | Posted: 11 December 2023 doi:10.20944/preprints202312.0733.v1

obviously stronger than the absolute value of $\Delta mlCRE_{TOAlw}$ over most low- and mid-latitude regions where solar radiation is relatively more dominant. Therefore, the $\Delta mlCRE_{TOA}$ ($\Delta mlCRE_{TOAlw}$ + $\Delta mlCRE_{TOAsw}$) from cirrus thinning simulations are positive over most low- and mid-latitude regions. Over the Western Pacific Warm Pool and nearby regions, the net warming effect (i.e., positive $\Delta mlCRE_{TOA}$) is considerable and statistically significant. The globally averaged $\Delta mlCRE_{TOA}$ from the HET and SEED simulations are 1.35 ± 0.18 and 1.25 ± 0.16 W m^{-2}, respectively. This warming effect caused by the alterations in mixed-phase and liquid clouds would counteract, to some extent, the cooling effect derived from the thinning of cirrus clouds alone (−3.56 ± 0.04 and −2.46 ± 0.04 W m^{-2}). The next paragraph will analyze this influence. The globally averaged $\Delta mlCRE_{bri}$ from the HET and SEED simulations are 3.05 ± 0.25 and 2.50 ± 0.21 W m^{-2}, respectively. The brightening effect from mixed-phase and liquid clouds is a little larger than from cirrus clouds (2.78 ± 0.03 and 2.19 ± 0.03 W m^{-2}). In short, after implementing the cirrus thinning approach, the cooling and dimming effects of mixed-phase and liquid clouds become weaker. This is consistent with the decrease in mlCOD caused by cirrus thinning.

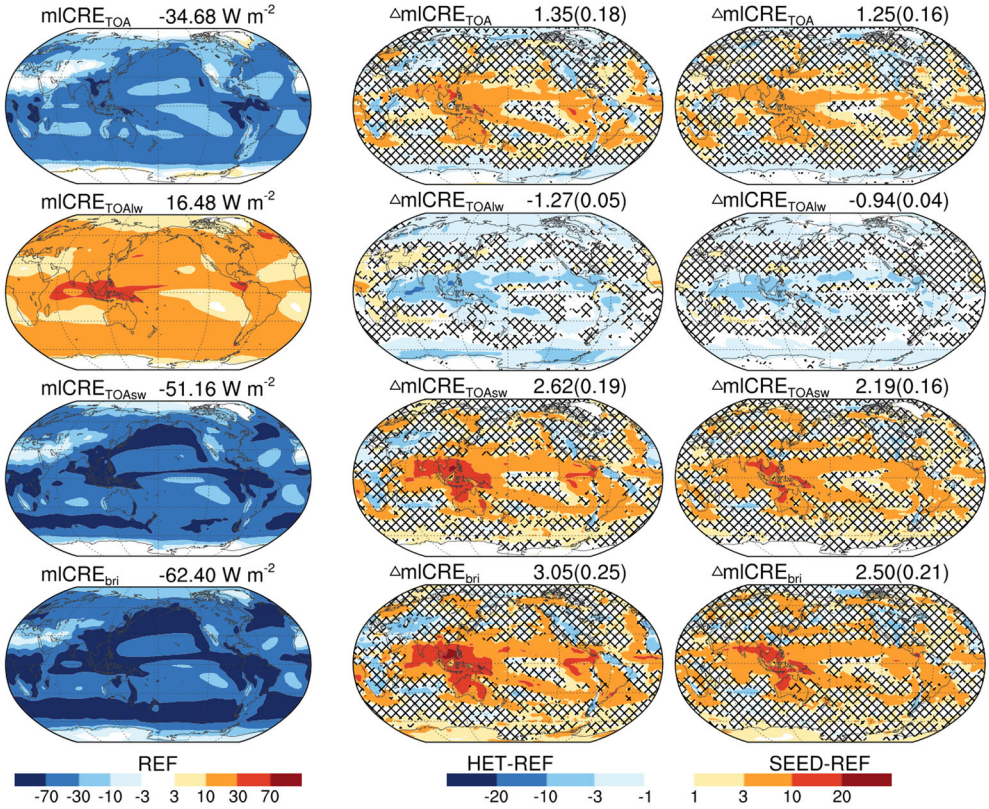

Figure 6. Similar to Figure 5, but for mixed-phase and liquid cloud radiative effect ($mlCRE_{TOA}$, $mlCRE_{TOAlw}$, $mlCRE_{TOAsw}$, and $mlCRE_{bri}$).

Finally, the brightening effect and cooling effect caused by cirrus thinning are quantified by the changes in radiative effects of entire clouds (ice, mixed-phase, and liquid clouds; Figure 7). In terms of solar radiation, the entire cloud has a globally averaged shortwave cooling effect (CRE_{TOAsw} is −56.42 W m^{-2}) and dimming effect (CRE_{bri} is −66.91 W m^{-2}). Cirrus thinning not only significantly decreases the shortwave cooling effect and dimming effect of cirrus clouds but also leads to substantial reductions (less negative in radiative effects) within the lower mixed-phase and liquid clouds. Hence, the entire cloud exhibits considerable reductions in both the shortwave cooling effect and the dimming effect. The globally averaged ΔCRE_{TOAsw} from HET and SEED simulations are 6.02 ± 0.21 and 4.85 ± 0.17 W m^{-2}, respectively. The globally averaged ΔCRE_{bri} from the HET and SEED simulations are 5.83 ± 0.26 and 4.69 ± 0.21 W m^{-2}, respectively. The brightening effect (i.e., positive ΔCRE_{bri}) is close to the shortwave warming effect (positive ΔCRE_{TOAsw}), and they have a similar spatial pattern. The ΔCRE_{bri} are predominantly significant across most low- and mid-latitude regions,

Preprints (www.preprints.org) | NOT PEER-REVIEWED | Posted: 11 December 2023 doi:10.20944/preprints202312.0733.v1

primarily attributable to the intense solar radiation present in these areas. In terms of longwave radiation, the cloud has a global averaged warming effect (CRE_{TOAlw} is 28.27 W m^{-2}). Although the globally averaged CRE_{TOAlw} is roughly half of the absolute value of CRE_{TOAsw}, ΔCRE_{TOAlw} is generally stronger than ΔCRE_{TOAsw} due to the dominant contribution from cirrus clouds (i.e., $\Delta iCRE_{TOAlw}$). In terms of the sum of shortwave and longwave radiation, the cloud has a globally averaged cooling effect (CRE_{TOA} is −28.15 W m^{-2}). The ΔCRE_{TOA} caused by cirrus thinning also shows cooling effect. The ΔCRE_{TOA} from the HET and SEED simulations are −2.21 ± 0.18 and −1.21 ± 0.19 W m^{-2}, respectively. Unlike the brightening effect, the cooling effect (i.e., negative ΔCRE_{TOA}) is statistically significant over most high-latitude regions because solar radiation is weak at high latitudes. In comparison to artificially halting homogeneous nucleation (i.e., the HET simulation), the globally averaged cooling effect resulting from the seeding method decreases by approximately half. Unlike the cooling effect, the relative reduction of the brightening effect is considerably less, falling by about one-fourth. In the SEED simulation, the globally averaged brightening effect is approximately four times stronger than the globally averaged cooling effect. This suggests that cirrus thinning via seeding INPs not only cools our planet but also provides much stronger brightening effect.

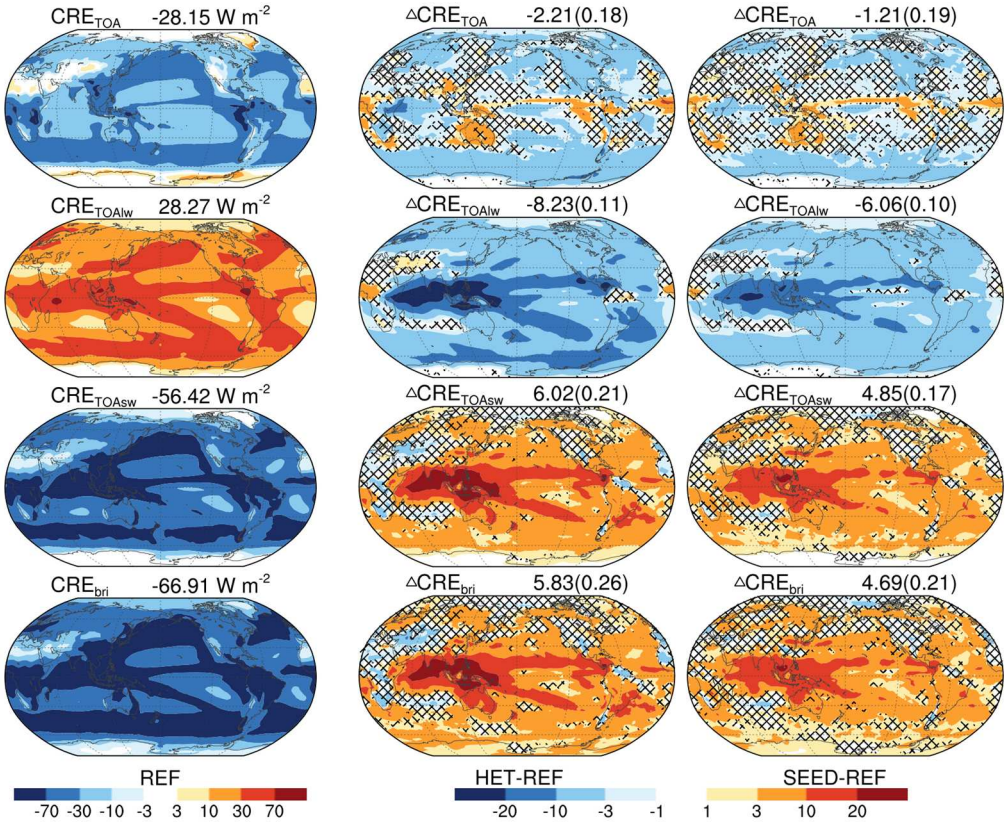

Figure 7. Similar to Figure 5, but for the entire clouds (ice, mixed-phase, and liquid) radiative effect (CRE_{TOA}, CRE_{TOAlw}, CRE_{TOAsw}, and CRE_{bri}).

4. Discussion

Compared to artificially halting homogeneous nucleation (i.e., the HET simulation) or artificially increasing the fall velocity of ICs (e.g., GeoMIP6), cirrus thinning via seeding INPs holds potential real-world feasibility. Whether there is a need to seed INPs (i.e., if $N_{INP} < N_{INPlim}$) and the quantity of INPs to be seeded (i.e., $N_{INPseed}$) depend on the ambient atmospheric condition. The $N_{INPseed}$ over different locations/times are different. Even if the $N_{INPseed}$ has been accurately calculated, a significant number of aircraft would be needed to seed these INPs at specific times and locations. This logistical challenge presents the main barrier to the real-world feasibility of cirrus thinning. From this perspective, the SEED simulation remains largely an academic endeavor. While the quantified values of the brightening effect shown in this study are important, the analyses exploring the mechanisms

 doi:10.20944/preprints202312.0733.v1

behind this brightening effect are arguably more robust and useful. These mechanism analyses could potentially contribute to future technological developments in geoengineering.

5. Conclusions

This study investigates the brightening effect caused by cirrus thinning with CAM5 model. Here, two methods are used for cirrus thinning: artificially halting homogeneous nucleation (HET simulation) and hindering homogeneous nucleation via seeding a few INPs (SEED simulation). As anticipated, the SEED simulation exhibits marginally diminished alterations in cloud radiative effects when compared to those from the HET simulation. Nevertheless, the underlying mechanism driving these changes remains consistent. For cirrus thinning simulations through the reduction of homogeneous nucleation, this mechanism appears to be more robust. The following conclusions drawn are primarily based on the SEED simulation results, which possess better reference values.

After seeding INPs, both N_{inuc} and N_i are significantly reduced to a very low level. The IWC of cirrus clouds is also noticeably decreased. These result in a reduction of cirrus COD (both $iCOD_{lw}$ and $iCOD_{sw}$) by approximately half. Consequently, the net warming effect (positive $iCRE_{TOA}$, $iCRE_{TOA}$ = $iCRE_{TOAlw}$ + $iCRE_{TOAsw}$) and dimming effect (negative $iCRE_{bri}$, $iCRE_{bri}$ is close to $iCRE_{TOAsw}$) from these cirrus clouds are reduced by approximately half. Both the cooling effect (negative $\Delta iCRE_{TOA}$, -2.46 ± 0.04 W m^{-2}) and brightening effect (positive $\Delta iCRE_{bri}$, 2.19 ± 0.03 W m^{-2}) induced by cirrus thinning alone (i.e., only the changes in cirrus clouds) are significant. In addition, cirrus thinning also results in substantial reductions in the COD of mixed-phase and liquid clouds over some regions. Correspondingly, the net cooling effect (i.e., negative $mlCRE_{TOA}$) and dimming effect (i.e., negative $mlCRE_{bri}$, $mlCRE_{bri}$ is close to $mlCRE_{TOAsw}$) from these mixed-phase and liquid clouds are also reduced. In other words, the changes within mixed-phase and liquid clouds induced by cirrus thinning lead to a globally averaged warming effect ($\Delta mlCRE_{TOA}$, 1.25 ± 0.16 W m^{-2}) and brightening effect ($\Delta mlCRE_{bri}$, 2.50 ± 0.21 W m^{-2}). This warming effect (i.e., $\Delta mlCRE_{TOA}$) counteracts the cooling effect from the thinning of cirrus clouds alone (i.e., $\Delta iCRE_{TOA}$), whereas this brightening effect (i.e., $\Delta mlCRE_{bri}$) enhances the brightening effect from cirrus clouds (i.e., $\Delta iCRE_{bri}$). Therefore, the overall brightening effect (4.69 ± 0.21 W m^{-2}) induced by seeding INPs is much more pronounced than its cooling effect (-1.21 ± 0.19 W m^{-2}).

The spatial distribution of the brightening effect differs from that of the cooling effect due to the weakening of solar radiation at high latitudes. Cirrus thinning simulations demonstrate a significant cooling effect (negative ΔCRE_{TOA} in Figure 7) over most high-latitude regions. This spatial distribution pattern is more conducive to mitigating the melting of polar ice caps and glaciers. Contrary to the cooling effect, the brightening effect (positive ΔCRE_{bri} in Figure 7) is considerable over most low- and mid-latitude regions. If implementing marine cloud brightening (another geoengineering approach) over the Western Pacific Warm Pool and adjacent regions, the reduction in Earth's surface brightness due to increased marine cloud COD could potentially be offset by the cirrus seeding approach. In short, the cirrus thinning approach possesses a unique advantage (i.e., the brightening effect) that other geoengineering approaches lack. Integrating the cirrus seeding with other geoengineering approaches could potentially enhance the cooling effect and reduce side effects [84].

Author Contributions: X.S. designed this study. X.S. and J.L. modified CAM5 model code. Y.L. carried out parcel model simulations and CAM5 simulations. X.S. and Y.L. analyzed simulation results and wrote the manuscript. All authors have read and agreed to the published version of the manuscript.

Funding: This research was funded by the National Natural Science Foundation of China (grant nos. 41775095 and 42075145). The APC was supported by the same funders.

Institutional Review Board Statement: Not applicable.

Informed Consent Statement: Not applicable.

Data Availability Statement: The Fortran code for cloud parcel model, modified CAM5 model code, the NCL scripts and simulation results used for making plots have been archived in a public repository (https://doi.org/10.5281/zenodo.10261111, accessed on 5 December 2023).

Acknowledgments: This study was conducted at the High-Performance Computing Center of Nanjing University of Information Science and Technology.

Conflicts of Interest: The authors declare no conflicts of interest.

References

1. Zhang, J.C.; Zhang, K.; Liu, J.F.; Ban-Weiss, G. Revisiting the climate impacts of cool roofs around the globe using an Earth system model. *Environ. Res. Lett.* **2016**, *11*, 084014, doi:10.1088/1748-9326/11/8/084014.
2. IPCC. Global Warming of 1.5°C. An IPCC Special Report on the impacts of global warming of 1.5°C above pre-industrial levels and related global greenhouse gas emission pathways, in the context of strengthening the global response to the threat of climate change, sustainable development, and efforts to eradicate poverty; Masson-Delmotte, V., Zhai, P., Pörtner, H.-O., Roberts, D., Skea, J., Shukla, P.R., Pirani, A., Moufouma-Okia, W., Péan, C., Pidcock, R., Eds.; Cambridge University Press: Cambridge, United Kingdom and New York, NY, USA, 2018, doi:10.1017/9781009157940.
3. Vaughan, N.E.; Gough, C.; Mander, S.; Littleton, E.W.; Welfle, A.; Gernaat, D.E.H.J.; van Vuure, D.P. Evaluating the use of biomass energy with carbon capture and storage in low emission scenarios. *Environ. Res. Lett.* **2018**, *13*, 044014, doi:10.1088/1748-9326/aaaa02.
4. Gruber, S.; Blahak, U.; Haenel, F.; Kottmeier, C.; Leisner, T.; Muskatel, H.; Storelvmo, T.; Vogel, B. A process study on thinning of Arctic winter cirrus clouds with high-resolution ICON-ART simulations. *J. Geophys. Res. Atmos.* **2019**, *124*, 5860–5888, doi:10.1029/2018JD029815.
5. Kravitz, B.; MacMartin, D.G.; Visioni, D.; Boucher, O.; Cole, J.N.S.; Haywood, J.; Jones, A.; Lurton, T.; Nabat, P.; Niemeier, U.; Robock, A.; Séférian, R.; Tilmes, S. Comparing different generations of idealized solar geoengineering simulations in the Geoengineering Model Intercomparison Project (GeoMIP). *Atmos. Chem. Phys.* **2021**, *21*, 4231–4247, doi:10.5194/acp-21-4231-2021.
6. Diamond M.S.; Gettelman, A.; Lebsock M.D.; McComiskey, A.; Russell, L.M.; Wood, R.; Feingold, G. To assess marine cloud brightening's technical feasibility, we need to know what to study—and when to stop. *Proc. Natl. Acad. Sci. USA* **2022**, *119*, e2118379119, doi:10.1073/pnas.2118379119.
7. MacMartin, D.G.; Visioni, D.; Kravitz, B.; Richter, J.H.; Felgenhauer, T.; Lee, W.R.; Morrow, D.R.; Parson, E.A.; Sugiyama, M. Scenarios for modeling solar radiation modification. *Proc. Natl. Acad. Sci. USA* **2022**, *119*, e2202230119, doi:10.1073/pnas.2202230119.
8. Baur, S.; Nauels, A.; Nicholls, Z.; Sanderson, B.M.; Schleussner, C.-F. The deployment length of solar radiation modification: an interplay of mitigation, net-negative emissions and climate uncertainty. *Earth Syst. Dynam.* **2023**, *14*, 367–381, doi:10.5194/esd-14-367-2023.
9. Caldeira, K.; Bala, G.; Cao, L. The Science of Geoengineering. *Annu. Rev. Earth Planet. Sci.* **2013**, *41*, 231–256, doi:10.1146/annurev-earth-042711-105548.
10. Boucher, O.; Randall, D.; Artaxo, P.; Bretherton, C.; Feingold, G.; Forster, P.; Kerminen, V.M.; Kondo, Y.; Liao, H.; Lohmann, U.; et al. Clouds and Aerosols. In *Climate Change 2013: The Physical Science Basis. Contribution of Working Group I to the Fifth As-sessment Report of the Intergovernmental Panel on Climate Change*; Stocker, T.F., Qin, D., Plattner, G.K., Tignor, M., Allen, S.K., Boschung, J., Nauels, A., Xia, Y., Bex, V., Midgley, P.M., Eds.; Cambridge University Press: Cambridge, United Kingdom and New York, NY, USA, 2013; pp. 571–658, doi:10.1017/CBO9781107415324.016.
11. IPCC. Climate Change 2014: Mitigation of Climate Change. Contribution of Working Group III to the Fifth Assessment Report of the Intergovernmental Panel on Climate Change; Edenhofer, O., Pichs-Madruga, R., Sokona, Y., Farahani, E., Kadner, S., Seyboth, K., Adler, A., Baum, I., Brunner, S., Eickemeier, P., Eds.; Cambridge University Press: Cambridge, United Kingdom and New York, NY, USA, 2014, doi:10.1017/CBO9781107415416.
12. Irvine, P.J.; Kravitz, B.; Lawrence, M.G.; Muri, H. An overview of the Earth system science of solar geoengineering. Wiley Interdiscip. *Rev. Clim. Change* **2016**, *7*, 815–833, doi:10.1002/wcc.423.
13. Cao, L. Short commentary on CMIP6 Geoengineering Model Intercomparison Project (GeoMIP). *Clim. Change Res.* **2019**, *15*, 487–492, doi:10.12006/j.issn.1673-1719.2019.195.

14. IPCC. Climate Change 2021: The Physical Science Basis. Contribution of Working Group I to the Sixth Assessment Report of the Intergovernmental Panel on Climate Change; Masson-Delmotte, V., Zhai, P., Pirani, A., Connors, S.L., Péan, C., Berger, S., Caud, N., Chen, Y., Goldfarb, L., Gomis, M.I., Eds.; Cambridge University Press: Cambridge, United Kingdom and New York, NY, USA, 2021, doi:10.1017/9781009157896.
15. Keller, D.P.; Lenton, A.; Scott, V.; Vaughan, N.E.; Bauer, N.; Ji, D.; Jones, C.D.; Kravitz, B.; Muri, H.; Zickfeld, K. The Carbon Dioxide Removal Model Intercomparison Project (CDRMIP): rationale and experimental protocol for CMIP6. *Geosci. Model Dev.* **2018**, *11*, 1133–1160, doi:10.5194/gmd-11-1133-2018.
16. Minx, J.C.; Lamb, W.F.; Callaghan, M.W.; Fuss, S.; Hilaire, J.; Creutzig, F.; Amann, T.; Beringer, T.; de Oliveira Garcia, W.; Hartmann, J.; Khanna, T.; Lenzi, D.; Luderer, G.; Nemet, G.F.; Rogelj, J.; Smith, P.; Vicente Vicente, J.L.; Wilcox, J.; del Mar Zamora Dominguez, M. Negative emissions—Part 1: research landscape and synthesis. *Environ. Res. Lett.* **2018**, *13*, 063001, doi:10.1088/1748-9326/aabf9b.
17. Rickels, W.; Reith, F.; Keller, D.; Oschlies, A.; Quaas, M.F. Integrated Assessment of Carbon Dioxide Removal. *Earth's Future* **2018**, *6*, 565–582, doi:10.1002/2017EF000724.
18. Cao, L. Climate system response to carbon dioxide removal. *Clim. Change Res.* **2021**, *17*, 664–670, doi:10.12006/j.issn.1673-1719.2021.169.
19. Alterskjær, K.; Kristjánsson, J.E.; Seland, Ø. Sensitivity to deliberate sea salt seeding of marine clouds—observations and model simulations. *Atmos. Chem. Phys.* **2012**, *12*, 2795–2807, doi:10.5194/acp-12-2795-2012.
20. Keith, D.W.; MacMartin, D.G. A temporary, moderate and responsive scenario for solar geoengineering. *Nat. Clim. Change* **2015**, *5*, 201–206, doi:10.1038/nclimate2493.
21. Jones, A.C.; Hawcroft, M.K.; Haywood, J.M.; Jones, A.; Guo, X.; Moore, J.C. Regional Climate Impacts of Stabilizing Global Warming at 1.5 K Using Solar Geoengineering. *Earth's Future* **2018**, *6*, 230–251, doi:10.1002/2017EF000720.
22. Kravitz, B.; Rasch, P.J.; Wang, H.; Robock, A.; Gabriel, C.; Boucher, O.; Cole, J.N.S.; Haywood, J.; Ji, D.; Jones, A.; Lenton, A.; Moore, J.C.; Muri, H.; Niemeier, U.; Phipps, S.; Schmidt, H.; Watanabe, S.; Yang, S.; Yoon, J. The climate effects of increasing ocean albedo: an idealized representation of solar geoengineering. *Atmos. Chem. Phys.* **2018**, *18*, 13097–13113, doi:10.5194/acp-18-13097-2018.
23. Gasparini, B.; McGraw, Z.; Storelvmo, T.; Lohmann, U. To what extent can cirrus cloud seeding counteract global warming?. *Environ. Res. Lett.* **2020**, *15*, 054002, doi:10.1088/1748-9326/ab71a3.
24. Cao, L. Climate system response to solar radiation modification. *Clim. Change Res.* **2021**, *17*, 671–684, doi:10.12006/j.issn.1673-1719.2021.170.
25. Vaughan, N.E.; Lenton, T.M. A review of climate geoengineering proposals. *Clim. Change* **2011**, *109*, 745–790, doi:10.1007/s10584-011-0027-7.
26. Kravitz, B.; Robock, A.; Tilmes, S.; Boucher, O.; English, J.M.; Irvine, P.J.; Jones, A.; Lawrence, M.G.; MacCracken, M.; Muri, H.; Moore, J.C.; Niemeier, U.; Phipps, S.J.; Sillmann, J.; Storelvmo, T.; Wang, H.; Watanabe, S. The Geoengineering Model Intercomparison Project Phase 6 (GeoMIP6): simulation design and preliminary results. *Geosci. Model. Dev.* **2015**, *8*, 3379–3392, doi:10.5194/gmd-8-3379-2015.
27. Xin, Y. A Brief Review and Outlook of Geoengineering. *Adv. Meteor. Sci. Technol.* **2016**, *60*, 30–36, doi:10.3969/j.issn.2095-1973.2016.04.004.
28. Duan, L.; Cao, L.; Bala, G.; Caldeira K. Comparison of the fast and slow climate response to three radiation management geoengineering schemes. *J. Geophys. Res. Atmos.* **2018**, *123*, 11980–12001, doi:10.1029/2018JD029034.
29. Lawrence, M.G.; Schäfer, S.; Muri, H.; Scott, V.; Oschlies, A.; Vaughan, N.E.; Boucher, O.; Schmidt, H.; Haywood, J.; Scheffran, J. Evaluating climate geoengineering proposals in the context of the Paris Agreement temperature goals. *Nat. Commun.* **2018**, *9*, 3734, doi:10.1038/s41467-018-05938-3.
30. Shepherd, J.; Caldeira, K.; Cox, P.; Haigh, J.; Keith, D.; Launder, B.; Mace, G.; MacKerron, G.; Pyle, J.; Raynor, S.; Redgwell, C.; Watson, A. Geoengineering the Climate: Science, governance and uncertainty; The Royal Society Publishing: London, UK, 2009; ISBN 978-0-85403-773-5.
31. Fairbrother, M. Geoengineering, moral hazard, and trust in climate science: evidence from a survey experiment in Britain. *Clim. Change* **2016**, *139*, 477–489, doi:10.1007/s10584-016-1818-7.
32. Lohmann, U.; Gasparini, B. A cirrus cloud climate dial?. *Science* **2017**, *357*, 248–249, doi:10.1126/science.aan3325.
33. Heutel, G.; Moreno-Cruz, J.; Shayegh, S. Solar geoengineering, uncertainty, and the price of carbon. *J. Environ. Econ. Manage.* **2018**, *87*, 24–41, doi:10.1016/j.jeem.2017.11.002.

34. Pezzoli, P.; Emmerling, J.; Tavoni, M. SRM on the table: the role of geoengineering for the stability and effectiveness of climate coalitions. *Clim. Change* **2023**, *176*, 1-21, doi:10.1007/s10584-023-03604-2.
35. Naik, V.; Wuebbles, D.; DeLucia, E.; Foley J.A. Influence of Geoengineered Climate on the Terrestrial Biosphere . *Environ. Manage.* **2003**, *32*, 373–381, doi:10.1007/s00267-003-2993-7.
36. Robock, A.; Marquardt, A.; Kravitz, B.; Stenchikov, G. Benefits, risks, and costs of stratospheric geoengineering. *Geophys. Res. Lett.* **2009**, *36*, L19703, doi:10.1029/2009GL039209.
37. Pitari, G.; Aquila, V.; Kravitz, B.; Robock, A.; Watanabe, S.; Cionni, I.; Luca, N.D.; Genova, G.D.; Mancini, E.; Tilmes, S. Stratospheric ozone response to sulfate geoengineering: Results from the Geoengineering Model Intercomparison Project (GeoMIP). *J. Geophys. Res. Atmos.* **2014**, *119*, 2629–2653, doi:10.1002/2013JD020566.
38. Kleidon, A.; Kravitz, B.; Renner, M. The hydrological sensitivity to global warming and solar geoengineering derived from thermodynamic constraints. *Geophys. Res. Lett.* **2015**, *42*, 138–144, doi:10.1002/2014GL062589.
39. Zarnetske, P.L.; Gurevitch, J.; Franklin, J.; Groffman, P.M.; Harrison, C.S.; Hellmann, J.J.; Hoffman, F.M.; Kothari, S.; Robock, A.; Tilmes, S.; Visioni, D.; Wu, J.; Xia, L.; Yang, C.E. Potential ecological impacts of climate intervention by reflecting sunlight to cool Earth. *Proc. Natl. Acad. Sci. USA* **2021**, *118*, e1921854118, doi:10.1073/pnas.1921854118.
40. Tye, M.R.; Dagon, K.; Molina, M.J.; Richter, J.H.; Visioni, D.; Kravitz, B.; Tilmes, S. Indices of extremes: geographic patterns of change in extremes and associated vegetation impacts under climate intervention. *Earth Syst. Dynam.* **2022**, *13*, 1233–1257, doi:10.5194/esd-13-1233-2022.
41. Jones, A.C.; Haywood, J.M.; Dunstone, N.; Emanuel, K.; Hawcroft, M.K.; Hodges, K.I.; Jones, A. Impacts of hemispheric solar geoengineering on tropical cyclone frequency. *Nat. Commun.* **2017**, *8*, 1382, doi:10.1038/s41467-017-01606-0.
42. Kristjánsson, J.E.; Muri, H.; Schmidt, H. The hydrological cycle response to cirrus cloud thinning. *Geophys. Res. Lett.* **2015**, *42*, 10807–10815, doi:10.1002/2015GL066795.
43. Liu, J.; Shi, X. Estimating the potential cooling effect of cirrus thinning achieved via the seeding approach. *Atmos. Chem. Phys.* **2021**, *21*, 10609–10624, doi:10.5194/acp-21-10609-2021.
44. Pongratz, J.; Lobell, D.B.; Cao, L.; Caldeira, K. Crop yields in a geoengineered climate. *Nat. Clim. Chang.* **2012**, *2*, 101–105, doi:10.1038/nclimate1373.
45. Xia, L.; Robock, A.; Cole, J.; Curry, C.L.; Ji, D.; Jones, A.; Kravitz, B.; Moore, J.C.; Muri, H.; Niemeier, U.; Singh, B.; Tilmes, S.; Watanabe, S.; Yoon J. Solar radiation management impacts on agriculture in China: a case study in the Geoengineering Model Intercomparison Project (GeoMIP). *J. Geophys. Res. Atmos.* **2014**, *119*, 8695–8711, doi:10.1002/2013JD020630.
46. Parkes, B.; Challinor, A.; Nicklin, K. Crop failure rates in a geoengineered climate: impact of climate change and marine cloud brightening. *Environ. Res. Lett.* **2015**, *10*, 084003, doi:10.1088/1748-9326/10/8/084003.
47. Zhan, P.; Zhu, W.Q.; Zhang, T.Y.; Cui, X.F.; Li, N. Impacts of sulfate geoengineering on rice yield in China: Results from a multimodel ensemble. *Earth's Future* **2019**, *7*, 395–410, doi:10.1029/2018EF001094.
48. Fan, Y.; Tjiputra, J.F.; Muri, H.; Lombardozzi, D.L.; Park, C.; Wu, S.; Keith, D. Solar geoengineering can alleviate climate change pressures on crop yields. *Nat. Food* **2021**, *2*, 373–381, doi:10.1038/s43016-021-00278-w.
49. Kravitz, B. Effects of climate engineering on agriculture. *Nat. Food* **2021**, *2*, 320–321, doi:10.1038/s43016-021-00277-x.
50. Proctor, J. Atmospheric opacity has a nonlinear effect on global crop yields. *Nat. Food* **2021**, *2*, 166–173, doi:10.1038/s43016-021-00240-w.
51. Wanser, K.; Doherty, S.J.; Hurrell, J.W.; Wong, A. Near-term climate risks and solar radiation modification: a roadmap approach for physical sciences research. *Clim. Change* **2022**, *174*, 23, doi:10.1007/s10584-022-03446-4.
52. Cassidy, M.; Sandberg, A.; Mani, L. The ethics of volcano geoengineering. *Earth's Future* **2023**, *11*, e2023EF003714, doi:10.1029/2023EF003714.
53. Kortetmäki, T.; Oksanen, M. Right to Food and Geoengineering. *J. Agric. Environ. Ethics* **2023**, *36*, 1–17, doi:10.1007/s10806-023-09898-7.
54. McDonald, M. Geoengineering, climate change and ecological security. *Env. Polit.* **2023**, *32*, 565–585, doi:10.1080/09644016.2022.2113606.

55. Berry, E.; Mace, G.G. Cloud properties and radiative effects of the Asian summer monsoon derived from A-Train data. *J. Geophys. Res. Atmos.* **2014**, *119*, 9492–9508, doi:10.1002/2014JD021458.
56. Hong, Y.; Liu, G.; Li, J.F. Assessing the Radiative Effects of Global Ice Clouds Based on CloudSat and CALIPSO Measurements. *J. Clim.* **2016**, *29*, 7651–7674, doi:10.1175/JCLI-D-15-0799.1.
57. Matus, A.V.; L'Ecuyer, T.S. The role of cloud phase in Earth's radiation budget. *J. Geophys. Res. Atmos.* **2017**, *122*, 2559–2578, doi:10.1002/2016JD025951.
58. Storelvmo, T.; Herger, N. Cirrus cloud susceptibility to the injection of ice nuclei in the upper troposphere. *J. Geophys. Res. Atmos.* **2014**, *119*, 2375–2389, doi:10.1002/2013JD020816.
59. Gasparini, B.; Münch, S.; Poncet, L.; Feldmann, M.; Lohmann, U. Is increasing ice crystal sedimentation velocity in geoengineering simulations a good proxy for cirrus cloud seeding?. *Atmos. Chem. Phys.* **2017**, *17*, 4871–4885, doi:10.5194/acp-17-4871-2017.
60. Ji, D.; Fang, S.; Curry, C.L.; Kashimura, H.; Watanabe, S.; Cole, J.N.S.; Lenton, A.; Muri, H.; Kravitz, B.; Moore, J.C. Extreme temperature and precipitation response to solar dimming and stratospheric aerosol geoengineering. *Atmos. Chem. Phys.* **2018**, *18*, 10133–10156, doi:10.5194/acp-18-10133-2018.
61. Liu, J. Cooling the earth and Brighten the surface by cirrus thinning geoengineering. Presented at the GeoMIP Meeting, Online, June 2020.
62. Duan, L.; Cao, L.; Bala, G; Caldeira K. A model-based investigation of terrestrial plant carbon uptake response to four radiation modification approaches. *J. Geophys. Res. Atmos.* **2020**, *125*, e2019JD031883, doi:10.1029/2019JD031883.
63. Mercado, L.; Bellouin, N.; Sitch, S.; Boucher, O.; Huntingford, C.; Wild, M.; Cox, P.M. Impact of changes in diffuse radiation on the global land carbon sink. *Nature* **2009**, *458*, 1014–1017, doi:10.1038/nature07949.
64. Wild, M.; Roesch, A.; Ammann, C. Global dimming and brightening - evidence and agricultural implications. *CABI Rev.* **2012**, *7*, 1–7, doi:10.1079/PAVSNNR20127003.
65. Yang, H.Y.; Dobbie, S.; Ramirez-Villegas, J.; Feng, K.; Challinor, A. J.; Chen, B.; Gao, Y.; Lee, L.; Yin, Y.; Sun, L.X.; Watson, J.; Koehler, A.; Fan, T.T.; Ghosh, S. Potential negative consequences of geoengineering on crop production: A study of Indian groundnut. *Geophys. Res. Lett.* **2016**, *43*, 11786–11795, doi:10.1002/2016GL071209.
66. Proctor, J.; Hsiang, S.; Burney, J.; Burke M.; Schlenker W. Estimating global agricultural effects of geoengineering using volcanic eruptions. *Nature* **2018**, *560*, 480–483, doi:10.1038/s41586-018-0417-3.
67. Meng, Q.; Liu, B.; Yang, H.; Chen, X. Solar dimming decreased maize yield potential on the North China Plain. *Food Energy Secur.* **2020**, *9*, e235, doi:10.1002/fes3.235.
68. Pruppacher, H.; Klett, J. *Microphysics of Clouds and Precipitation*; Atmospheric and Oceanographic Sciences Library, Vol. 18; Springer, Dordrecht, 2010, doi:.10.1007/978-0-306-48100-0.
69. Shi, X.; Liu, X. Effect of cloud-scale vertical velocity on the contribution of homogeneous nucleation to cirrus formation and radiative forcing. *Geophys. Res. Lett.* **2016**, *43*, 6588–6595, doi:10.1002/2016GL069531.
70. Neale, R.B.; Gettelman, A.; Park, S.; Chen, C.-C.; Lauritzen, P.H.; Williamson, D.L.; Conley, A.J.; Kinnison, D.; Marsh, D.; Smith, A.K.; Vitt, F.M.; Garcia, R.; Lamarque, J.-F.; Mills, M.J.; Tilmes, S.; Morrison, H.; Cameron-Smith, P.; Collins, W.D.; Iacono, M.J.; Easter, R.C.; Liu, X.; Ghan, S.J.; Rasch, P.J.; Taylor, M.A. Description of the NCAR Community Atmosphere Model (CAM 5.0); NCAR/TN-486+STR, National Center for Atmospheric Research: Boulder, Co, USA, 2012, doi:10.5065/wgtk-4g06.
71. Morrison, H.; Gettelman, A. A New Two-Moment Bulk Stratiform Cloud Microphysics Scheme in the Community Atmosphere Model, Version 3 (CAM3). Part I: Description and Numerical Tests. *J. Clim.* **2008**, *21*, 3642–3659, doi:10.1175/2008JCLI2105.1.
72. Liu, X.; Penner, J.E. Ice nucleation parameterization for global models. *Meteorol. Z.* **2005**, *14*, 499–514, doi:10.1127/0941-2948/2005/0059.
73. Barahona, D.; Nenes, A. Parameterizing the competition between homogeneous and heterogeneous freezing in ice cloud formation – polydisperse ice nuclei. *Atmos. Chem. Phys.* **2009**, *9*, 5933–5948, doi:10.5194/acp-9-5933-2009.
74. Shi, X.; Liu, X.; Zhang, K. Effects of pre-existing ice crystals on cirrus clouds and comparison between different ice nucleation parameterizations with the Community Atmosphere Model (CAM5), *Atmos. Chem. Phys.* **2015**, *15*, 1503–1520, doi:10.5194/acp-15-1503-2015.
75. Shi, X.; Liu, X. Sensitivity study of anthropogenic aerosol indirect forcing through cirrus clouds with CAM5 using three ice nucleation parameterizations. *J. Meteorol. Res.* **2018**, *32*, 693–706, doi:10.1007/s13351-018-8011-z.

76. Lohmann, U.; Spichtinger, P.; Jess, S.; Peter, T.; Smit, H. Cirrus cloud formation and ice supersaturated regions in a global climate model. *Environ. Res. Lett.* **2008**, *3*, 045022, doi:10.1088/1748-9326/3/4/045022.
77. Kärcher, B.; Lohmann, U. A parameterization of cirrus cloud formation: Homogenous freezing of supercooled aerosols. *J. Geophys. Res.* **2002**, *107*, 4010, doi:10.1029/2001JD000470.
78. Storelvmo, T.; Kristjansson, J.E.; Muri, H.; Pfeffer, M.; Barahona, D.; Nenes, A. Cirrus cloud seeding has potential to cool climate. *Geophys. Res. Lett.* **2013**, *40*, 178–182, doi:10.1029/2012GL054201.
79. Hoose, C.; Möhler, O. Heterogeneous ice nucleation on atmospheric aerosols: a review of results from laboratory experiments. *Atmos. Chem. Phys.* **2012**, *12*, 9817-9854, doi:10.5194/acp-12-9817-2012.
80. Gasparini, B.; Lohmann, U. Why cirrus cloud seeding cannot substantially cool the planet. *J. Geophys. Res. Atmos.* **2016**, *121*, 4877–4893, doi:10.1002/2015JD024666.
81. Mitchell, D.L.; Finnegan, W. Modification of cirrus clouds to reduce global warming. *Environ. Res. Lett.* **2009**, *4*, 045102, doi:10.1088/1748-9326/4/4/045102.
82. Rapp, A.D.; Kummerow, C.D.; Fowler, L. Interactions between warm rain clouds and atmospheric preconditioning for deep convection in the tropics. *J. Geophys. Res. Atmos.* **2011**, *116*, D23210, doi:10.1029/2011JD016143.
83. Muench, S.; Lohmann, U. Developing a cloud scheme with prognostic cloud fraction and two moment microphysics for ECHAM-HAM. *J. Adv. Model. Earth Syst.* **2020**, *12*, e2019MS001824, doi:10.1029/2019MS001824.
84. Cao, L.; Duan, L.; Bala, G.; Caldeira, K. Simultaneous stabilization of global temperature and precipitation through cocktail geoengineering. *Geophys. Res. Lett.* **2017**, *44*, 7429–7437, doi:10.1002/2017GL074281.